This paper describes objective technical results and analysis. Any subjective views or opinions that might be expressed in the paper do not necessarily represent the views of the U.S. Department of Energy or the United States Government.

SAND2019-3947C

Design and Evaluation of Task-Specific Compressive Optical Systems

Brian J. Redman, Gabriel C. Birch, Charles F. LaCasse, Amber L. Dagel, Tu-Thach Quach, and Meghan Galiardi

Sandia National Laboratories, 1515 Eubank Blvd SE, Albuquerque, NM 87123, United States

ABSTRACT

Many optical systems are used for specific tasks such as classification. Of these systems, the majority are designed to maximize image quality for human observers; however, machine learning classification algorithms do not require the same data representation used by humans. In this work we investigate compressive optical systems optimized for a specific machine sensing task. Two compressive optical architectures are examined: an array of prisms and neutral density filters where each prism and neutral density filter pair realizes one datum from an optimized compressive sensing matrix, and another architecture using conventional optics to image the aperture onto the detector, a prism array to divide the aperture, and a pixelated attenuation mask in the intermediate image plane.

We discuss the design, simulation, and tradeoffs of these compressive imaging systems built for compressed classification of the MNSIT data set. To evaluate the tradeoffs of the two architectures, we present radiometric and raytrace models for each system. Additionally, we investigate the impact of system aberrations on classification accuracy of the system. We compare the performance of these systems over a range of compression. Classification performance, radiometric throughput, and optical design manufacturability are discussed.

Keywords: compressive sensing, compressive classification, task-specific, MNIST

1. INTRODUCTION

Previous works have demonstrated classification tasks performed with high accuracy on compressed signals.[1–3] Compressive sensing approaches have enabled the generation of optical systems that collect these lower-dimensional representations of data directly, while still enabling estimation of the originally sensed data. However, traditional compressive sensing does not utilize information about the performance of the ultimate task as a means of selecting the best measurements to be collected by a device. In past work, it was shown that task-specific information enables optimizing a compressive measurement matrix to achieve better performance of a classification task than traditional compressed sensing methods.

In this work we demonstrate two optical architectures to realize optimized compressive sensing matrices. The first architecture achieves compressive measurements through the use of an array of prisms and neutral density filters in an non-imaging design. Each prism and filter pair enable realizing one non-zero element within an optimized measurement matrix. The second architecture utilizes a more conventional approach, with a less complex prism array dividing the aperture into channels which are imaged onto an intermediate image plane. The sensing matrix weighting in the second architecture was achieved using a digital micromirror device (DMD) device in the intermediate image plane. These two architectures represent different approaches to realizing the same optimized measurement matrix. The positive and negative attributes of these approaches will be discussed throughout the work.

Fig. 1 shows a high level overview of realizing a sensing matrix as an optical component. The classification task chosen for this paper was classifying the digits of the MNIST dataset. The generation of task-specific compressive sensing matrices was established in previous work,[4] and is discussed briefly in Section 1.1. Section 2 discusses sampling object space, Section 2.1 and Section 2.2 discuss the creation of the optical components.

Further author information: (Send correspondence to B.J.R.)
B.J.R.: E-mail: bjredma@sandia.gov, Telephone: 1 505 284 6468

Sandia National Laboratories is a multimission laboratory managed and operated by National Technology & Engineering Solutions of Sandia, LLC, a wholly owned subsidiary of Honeywell International Inc., for the U.S. Department of Energy's National Nuclear Security Administration under contract DE-NA0003525.

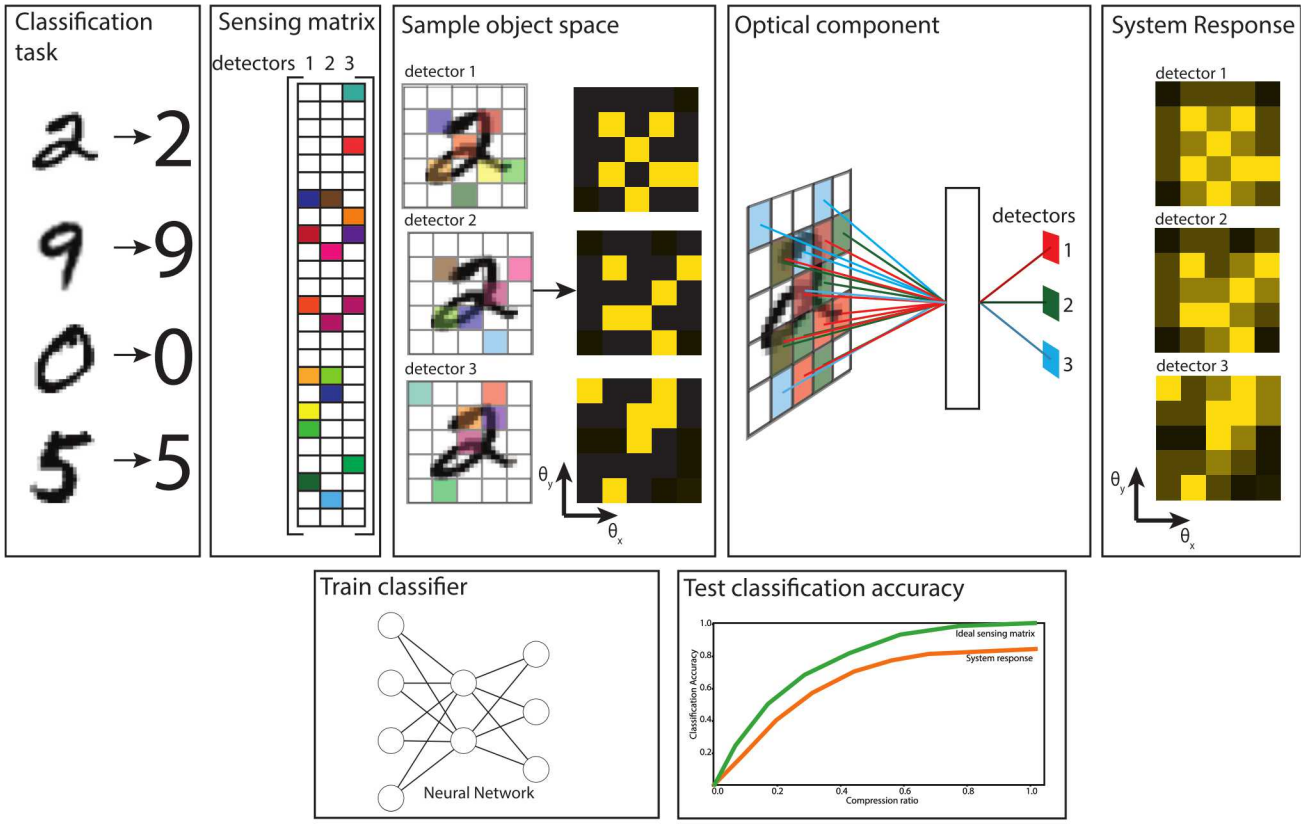

Figure 1. For task-specific compressive, a sensing matrix is created to reduce the dimensionality of the measurement. An optical component can be created from the sensing matrix by mapping the rows (input angles) to the columns (detectors). The system response matrices represent the optical component's sensitivity to input angles. The performance of the system is determined by how well a machine learning classifier can classify data compressed using the system response matrix.

Section 3.2 discusses the simulation of the system response. Section 4 presents the performance of the holistic optical device and algorithmic classifiers. The positive and negative attributes of each sensing architecture are discussed in Section 5. Finally, the conclusions and future work are discussed in Section 6.

1.1 Background

Classification of images is an active area of research for fields such as self driving cars,[5,6] facial recognition,[7] medical imaging,[8,9] and remote sensing.[10,11] In these fields the optical systems are performing a specific task, however the images are commonly optimized for a human observer. The classification of the images is performed using machine learning techniques which reduce the dimensionality of the data as part of the processing, therefore a smaller subset of data could be recorded without loss of performance. Compressive sensing focuses on recording the minimum amount of information while still maintaining high performance for a task such as object detection or classification.

Research in compressive sensing has shown that images can be reconstructed from datasets sampled below the Shannon-Nyquist sampling limit.[12] Being able to reconstruct the image indicates that the information is retained by the compressed images. It was shown that reconstruction of compressed images was not required for classification task performed using machine learning.[13,14] The concepts of compressive sensing and classification has been demonstrated in multiple experiments such as the Rice University single pixel compressive imager.[15,16]

Compressive sensing uses a sensing matrix to reduce the dimensionality of a set of data. Typically the matrix is random with a Gaussian or uniform distribution, which for many applications are near optimal. However work

has been done to further optimize the matrices.[17–20] For this work it is of particular interest to constrain the sensing matrix to be physically realizable as a physical optical element. In previous work, we have developed sensing matrices which are nonnegative and sparse,[4] and we reported initial simulation results for a physical realization of the sensing matrix using a prism array[21]

In this work we created a detailed simulation process which considers factors such as stray light, and present a new optical architecture to compare to the prism array.

2. OPTICAL DESIGNS

We designed optical systems to realize optimized measurement matrices as established by Birch et al.[4] for the MNIST task. These optical designs highly compress the data from the 784 pixels in the images to between one to nine measurements. Having so few detector elements reduces constraints on physical placement, detector co-location, and pixel size.

Both the images of the MNIST dataset and the sensing matrix are mathematical constructs which have to be translated to physical parameters to create an optical system. The image is assumed to be an object at an infinity, therefore the light from each pixel is a collimated source, or plane wave. The images in the MNIST dataset are 28 by 28 pixels, so the optical systems were designed for 28 by 28 input angles. The sensing matrix can be considered as a mapping of input angles in object space to detector values in image space. Each row of the sensing matrix is one input angle, and the column determines the detector. For a nonnegative sensing matrix, the weighting can be normalized to correspond to the transmission from each input angle.

The design problem was inherently under-defined because the images do not have physical properties such as size or radiant exitance. To make the problem tractable, we defined the source and detector geometry. With the object at infinity, the size was defined in angular space. We assumed a half field of view (HFOV) of 5°, corresponding to a fairly narrow field of view system. The size of the detectors was set to be 100 μm by 100 μm which is much larger than the pixels of a consumer camera. The small number of separated detectors allowed for larger detectors.

2.1 Prism Array Architecture

The sensing matrix maps values in object space to measurements in image space. Lenses cannot directly realize the mapping because lenses have a one-to-one mapping from input angle to output location, while each column of the sensing matrix has multiple separated nonzero values. Mapping multiple input angles to a single detector encourages the use of an array of elements. A prism is an element that maps an input angle to an output angle. If the position of the prism and detector are known, a prism maps an input angle to an output location. The transmission of the prism corresponds to the weighting of the sensing matrix. In this paper we discuss a process to design a prism array to realize an arbitrary sensing matrix. The process workflow is shown in Fig 2.

Before the prisms could be positioned, the position of the detectors had to be set because the prisms were clustered around the detectors. The separation between the detectors, and the distance between the prism array and the detector determined the stray-light between the prism arrays. This channel crosstalk could be decreased by widening the separation between the detectors, however a larger separation increased the size of the prism array. Decreasing the distance between the prism array and the detector decreased the required separation of the detectors, but increased the angle between the prisms and the detector. For this work, the separation between the detectors was set to 3 mm. The distance between the prism array and the detector was set to 9 mm.

With the detector positions set, each nonzero element in the sensing the prisms matrix was assigned a position on a grid centered on the corresponding detector. The grid spacing was determined by the size of the prisms. The size of the prism determined if the detector was under or over filled over the range of angles accepted by each prism. For this design, the prism size was set to 200 μm by 200 μm which overfills the detector for the designed field of view of each prism. The large prisms also increased the power on the detector at the expense of blurring the system response. The errors caused by the prism size relative to the detector size are discussed in more detail in Section 3.

The position of the prisms relative to the detector was used by a sequential raytrace program to optimize the angle of each prism. The index of refraction of the prism material was assumed to be 1.5 for all wavelengths.

The physical parameters of the prism array were used to create a physical model in a non-sequential raytracing program where each prism was modeled as a separate rectangular solid. The weighting of the sensing matrix was implemented with coating on the tilted surface of each prism. Transmissions were set to the weight of the normalized sensing matrix, and the reflectance was set to a uniform 6%. This was an approximation of neutral density filters where the reflection would be due to the glass filter interface, and the attenuation would be due to absorption inside the filter. It was also not feasible to implement the thousands transmissions with floating point precision, so the transmission values were uniformly binned into 128 values between 0 and 1. Raytraces through the non-sequential model were used to create the system response matrix of the prism array.

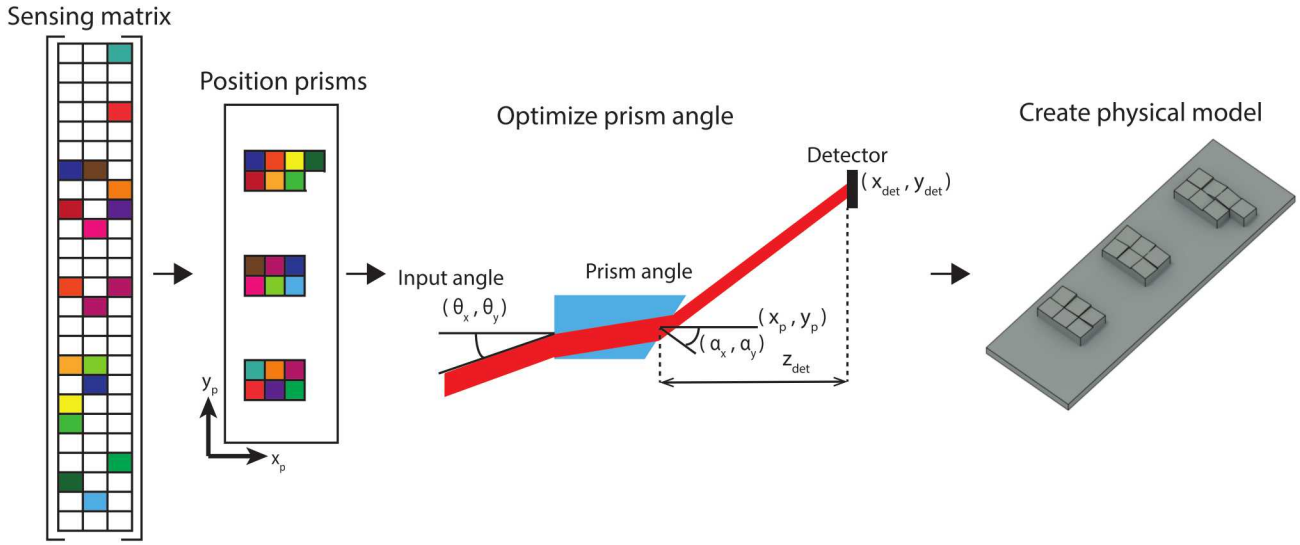

Figure 2. The prism array was created as a physical realization of the sensing matrix. First each nonzero entries from the sensing matrix was assigned to a physical location. Then the angles of each prism was optimized to map the input angle, determined by the location in the sensing matrix, to the detector position. A model was created from the prism geometry to allow for simulation of the optical system.

2.2 Digital Micromirror Device Architecture

The prism array requires many elements with small feature sizes and very sharp edges which is not feasible to fabricate using traditional methods. An alternative architecture using a digital micromirror device (DMD) and less complex prism array was created. This approach was tailored to enable the use of commercial off the shelf optical elements, and simple custom optical components. The DMD architecture presented in this work takes measurements simultaneous with parallel channels as opposed to the sequential measurements made by the Rice University single pixel compressive sensor.

To make parallel measurements required a channel for each detector which was spatially resolved at the DMD plane, but uniform irradiance at the detector plane. We achieved this using an objective lens to image the object onto the DMD plane and a relay lens to image the aperture onto the detector as shown in Fig. 3. The aperture was imaged onto the detector because the irradiance in the aperture is assumed to be uniform. The stop was located at the front focal point of the objective lens making the system telecentric, allowing the distance between the DMD and relay lens to be changed without any change of magnification.

The separate channels were formed using a prism array to divide the aperture. The angle of the prism set the separation between the channels in the intermediate image plane. Only one prism was required for each detector, and the size of the prisms were larger than the previous architecture allowing them to be fabricated as separate components using polishing techniques.

After the architecture was chosen, the parameters were optimized using paraxial optics as a proof of concept for the system, but each component was chosen to be possible to implement with commercial off the shelf

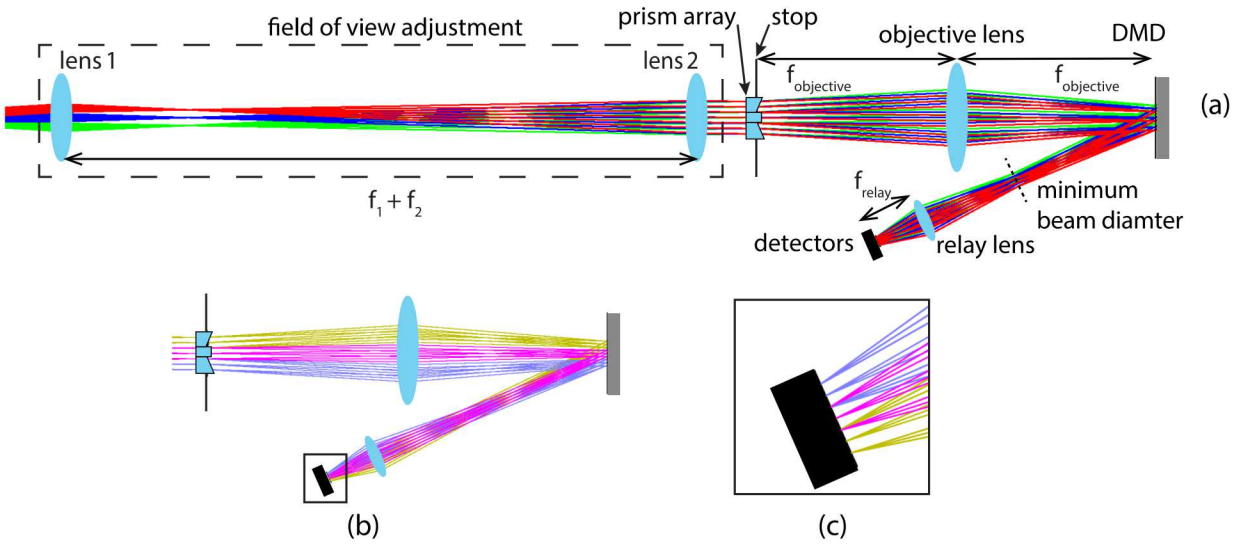

Figure 3. (a) The digital micomirror device (DMD) architecture uses a prism array to divide the stop. The object is imaged onto the DMD and the stop is imaged onto the detector. (b) Both the stop and the fields are separated at the DMD. (c) The fields are combined to be overlapping at the detector, but the channels are separated.

components. The first component set was the DMD, because the size of the DMD sets the requirements of the rest of the system. As a starting point, the design was created around the Texas Instruments® DLP® LightCrafter^{TM} 6500 which is a commercially available component with a large active area of 14.52 mm by 8.16 mm. There are 1920 by 1080 micromirrors across the active area, therefore the resolution of the DMD is much higher than the 28 by 28 pixels required for each channel. The channels on the DMD were arranged in a 3 by 3 grid, so the maximum size of each channel at the DMD plane was 2.72 mm by 2.72 mm. The light incident on the objective lens is collimated and images onto the DMD one focal length behind the objective lens, therefore the width of each channel at the DMD is,

$$w_{\text{channel}} = 2\tan(\text{HFOV}) f_{\text{objective}}, \tag{1}$$

where HFOV is the half field of view and $f_{\text{objective}}$ is the focal length of the objective lens. Using the 5° HFOV design constraint, requires the objective focal length to be less than 13.0 mm. The short focal length was not practical because the lens needed to be far enough away from the DMD that the reflection would not clip on the mounting hardware for the lens. Additionally, the size of the aperture imaged onto the detector plane is set by the ratio of the objective focal length to the relay focal length, and it is not reasonable to make the focal length of the relay lens significantly shorter than 13 mm.

A Keplerian telescope was added to the front of the system to maintain the 5° HFOV in object space and decrease the HFOV received by the objective lens. For the initial design, a HFOV magnification of 4 was chosen, so the HFOV received by the objective lens was 1.25° mm. With the reduced HFOV, the objective focal length needed to be less than 52.1 mm. Reducing the focal length to 50 mm allowed for more off the shelf solutions, and reduced the size of the channels at the DMD plane. The small unused region around each channel reduced the likelihood of channel crosstalk. With the focal length of the objective set, the angle of the prism was optimized to -5.85° for a 2.58 mm separation between the channels at the DMD. The separation smaller than 2.72 mm increased the unused pixels around the outside edge.

The beam for each channel was narrowest at the DMD. After that each beam expanded but the centers of the beams crossed. The centers of the beams converging creates a point where the total beam diameter is narrowest. The location and diameter where the narrowest beam diameter was determined by a combination of the field of view, prism angle, and objective lens focal length. In this design the relay lens was located farther from the

DMD than the minimum beam diameter because the minimum beam diameter was very close to the objective lens as seen in Fig 3 (b). The close proximity of the two lenses would not allow for mounting hardware.

The focal length of the relay lens was set to 5 mm to give a 10 times magnification of the detector area. The larger the magnification, the larger effective detector area at the aperture and therefore a greater throughput. However, the entrance pupil of the relay lens needed to be to be larger than the beam diameter therefore decreasing the focal length required a faster lens. Additionally, increasing the effective area of the detector requires a larger prism size or the prism will under fill the detector. Increasing the prism size also increases the beam diameter. For this work, the prisms were set to 4 mm by 4 mm which required a relay lens entrance pupil diameter of 11.7 mm, requiring an F/0.43 lens which is not feasible. However, if the size of the prisms was reduced to 1 mm by 1 mm (the effective size of the detector at the prism plane), the beam diameter at the relay lens was 3.59 mm requiring a F/1.39 lens, which is a commercially off the shelf option. More work will be done on developing an optimization process to increase the prism size and maximize the throughput of the system while using reasonable lenses.

The relay lens imaged the aperture onto the detectors. The detectors for this design were located in a 3 by 3 grid at the rear focal length of the relay lens with no separation between the detectors. For the cases of using fewer than nine detectors, the unused sections of the DMD would be set to no transmission. Therefore, no hardware changes were required for changing the number of measurements made.

3. ANALYSIS

A radiometric model was used to determine if enough power would be transmitted to the detector for the systems to work. Then a raytrace simulation was then used to analyze errors in the system which changed the system response matrix. The system response matrix compressed images of the MNIST data, and the performance of the system was measured from the accuracy with which a classifier could determine the digits. Aberrations were induced in the system to test how non-ideal optics will affect the system performance.

3.1 RADIOMETRIC MODEL

Radiometric throughput is used to calculate the signal power on the detector for a given source radiance, and enables analysis of the proposed compressive optical systems expected sensitivity requirements as compared to traditional imaging systems. In a traditional imaging device, the throughput can be defined by the area of the pixel and the projected solid angle subtended by the exit pupil. The compressive sensing systems are not imaging systems which makes calculating the throughput less straightforward.

Throughput can be calculated at any surface in the optical system, however, these calculations can be complex. In order to simplify this, we assume irradiance is constant at the aperture. In both of the compressive classification architectures, the aperture surface is at the prism array. The area in the throughput calculation is the effective area of the detector at the prism plane, and the projected solid angle is the summation of the instantaneous fields of view of each element weighted by the sensing matrix.

The effective area of the detector is calculated by projecting the detector to the plane of the prism array. In the DMD architecture, the aperture and detectors are conjugate planes, so the detectors can be projected onto the aperture plane using the magnification. For the prism array architecture, there is no magnification. The effective area is the detector area provided the beam from the prism fills the detector over the instantaneous field of view of the prism element. If the beam underfills the detector, the effective area is the illuminated portion of the detector which can be angle dependent. For both architectures, the effective area of the detector has to be compared to the area of the contributing prism, and the smaller of the two areas defines the aperture area.

The projected solid angle for the compressive sensing systems must be weighted by the sensing matrix. Therefore, the projected instantaneous field of view (iFOV) has to be calculated for each input angle. In this work, the iFOV was defined as the angle subtended by one of the 28 by 28 pixels in object space. For the DMD architecture, the HFOV was multiplied by the field of view magnification from the telescope.The projected solid angle was approximated as the differential solid angle times the cosine of the center angle. The approximation

was valid because the iFOV is small and the cosine of the largest input angle is proximately one. A differential solid angle can be calculated by the differential area that subtends it,

$$d\omega = \frac{dA}{r^2}, \tag{2}$$

where $d\omega$ is the differential solid angle, dA is the differential area, and r is the distance to the area. From this equation, if we set the distance to one and assume a rectangle defined by the pixel in angular space,

$$iFOV \approx d\omega \approx 4\tan\left(\frac{\theta_{\text{iFOV}}}{2}\right)^2, \tag{3}$$

where θ_{iFOV} is the apex angle that defines the iFOV. The projected solid angle of each input angle was weighted by the normalized sensing matrix. Then the throughput is the sum of the weighted projected solid angles times the effective area.

For the nine detector configuration, the throughputs of the prism array ranged from 2.1×10^{-12}m^{2}sr to 8.2×10^{-12}m^{2}sr. The DMD architecture ranged from 1.3×10^{-11}m^{2}sr to 5.1×10^{-11}m^{2}sr. For perspective, the throughput of a camera with an F/4 lens and 5 μm pixels is 1.2×10^{-12}m^{2}sr, which is less than prism array architecture.

3.2 Non-sequential Raytracing

The error caused by blurring can be analytically calculated, however it is not feasible to analytically calculate scattering and stray-light across the many element designs presented in this work. In order to evaluate the performance of the holistic compressive architectures performing an MNIST classification task, a raytrace was performed using Zemax Opticstudio®(ZOS). A source rectangle was added before the first surface of each design. The source created 10^6 randomly positioned collimated rays simulating the input from one object space location. The position and size of the source was set to fill the apertures of each system. To build up the system response matrix, flux on each detector was recorded for each input angle. For the MNIST data set there are 28 by 28 input angles, requiring 784 total raytraces.

It was not feasible to manually set each input angle, so we created an automatic process to build up the system response. The input angle was scanned using Python scripts controlling ZOS through the programs application programing interface (API). The flux on the detectors for each angle were saved into a matrix. The matrix was normalized to convert it into a system response matrix. The system response matrix was then used to simulate the optical system by multiplying the data before it was passed into a machine learning classifier.

3.3 Aberrations

Traditional quality metrics such as the point spread function or waves of aberrations do not directly translate to system performance of a compressive classification system. The best way to test how aberrations effect the classification accuracy of the holistic task-specific compressive classifier is to introduce aberrations in each system. This simulation is important especially for the DMD based architecture, because all the optics are parxial. If the systems are tolerant to aberrations then the lenses can be made up of fewer elements which reduces the weight and expense of the system.

The aberrations were induced using a high index plate placed directly before the prism array in each system. The rear surface sag of the plate was defined by Zernike polynomials. For a single wavelength, changing the sag of the surface causes a phase difference, inducing an aberration. The plate had a refractive index of 4 so that there would be minimal change in shape even for large aberrations. Zernike coefficients were set to achieve specific values of aberrations in terms of waves of Seidel aberrations. The system response matrix was generated for each aberration value to determine the effect the aberration had on system performance.

4. RESULTS AND DISCUSSION

The system response matrices of each system were created using the raytrace simulation procedures described previously. Example system response matrices for the case of nine detectors are shown in Fig. 4. For a perfect optical system, the system response matrices would exactly match the sensing matrix that they were designed from (i.e., the ideal sensing matrix shown in Fig. 4 (a) would be perfectly reproduced using the optical hardware). However, this was not the case; the prism array architecture raytraces show a highly blurred system response matrix compared to the ideal case. This blurring is caused by the beams from each prism overfilling the detectors. The DMD optical system closely reproduced the original system response matrix. However, there are rows and columns where the response was zero (e.g., a column of data is lost in Fig. 5 (c), k=5 detector response). This zero response results from regions where input angles focused directly on the edge of a DMD mirror in the simulation. The error would likely be removed for a real system with an iFOV instead of perfectly collimated light, however the error indicates that scattering will be a possible problem.

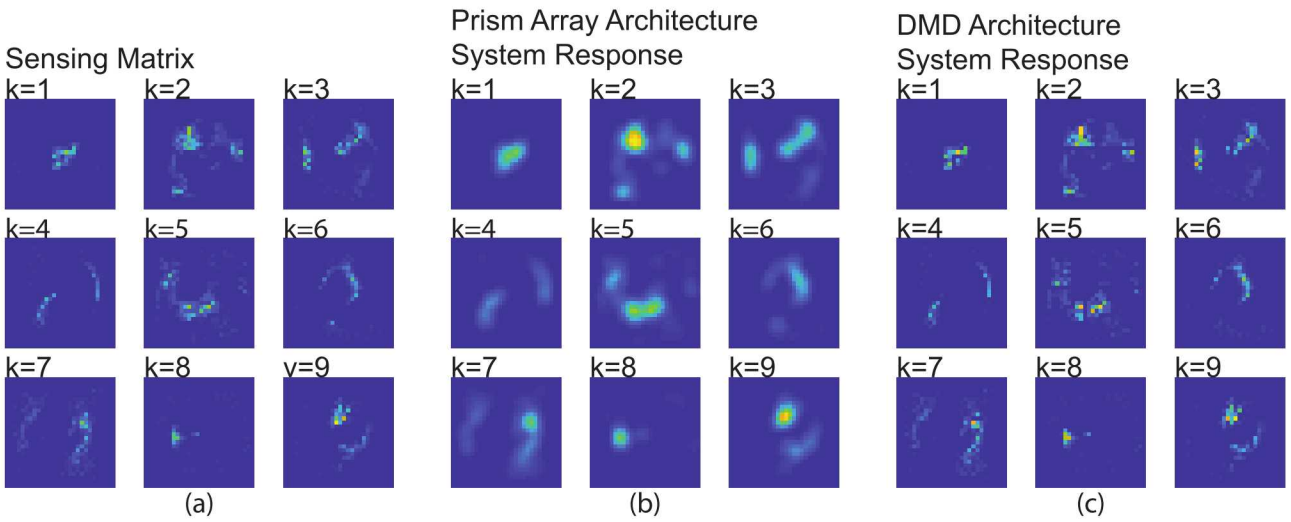

Figure 4. Side by side comparisons between the system response matrices for the nine detector configuration for the (a) ideal system response matrix, for the (b) prism array architecture, and for the (c) digital micromirror device (DMD) architecture.

The simulated system response matrices from raytrace simulation were used to compress the images from the MNIST dataset. A random-forest classifier was re-trained on the data. The re-trained classifier was then used to classify a compressed test dataset, and the classification accuracy was recorded. The training and classifying was repeated for ten random datasets to determine the classification accuracy mean and variance. The accuracy of the compressive sensing systems was compared to the classification accuracy when the sensing matrix was used to compress the data.

Fig. 5 shows the classification accuracy over a range of one to nine detectors, the error bars are set by the variance from ten training classification cycles. Both optical systems had very similar performance to the ideal sensing matrix, converging to over 90% accuracy using nine detectors (Fig. 5 (a)), and less than 3% difference for all the detectors (Fig. 5 (b)). The performance difference between the ideal sensing matrix and system response matrices (Fig. 5 (b)) showed the interesting result that the prism array had better performance than the ideal sensing matrix when a five, eight, or nine detector configuration was used. The prism array had significant blurring as seen in Fig. 4 (b). We expect blurring released some of the sparse constraint, allowing for improved performance without increase the number of prism elements. This indicates that classical design techniques may not be the best route for optimizing the compressive sensing systems. The below ideal performance of the DMD optical design was likely due to the dead rows and columns caused by an input angle being focused onto the edge of a DMD, and the system performance would likely be improved by simulating the full iFOV instead of a collimated source.

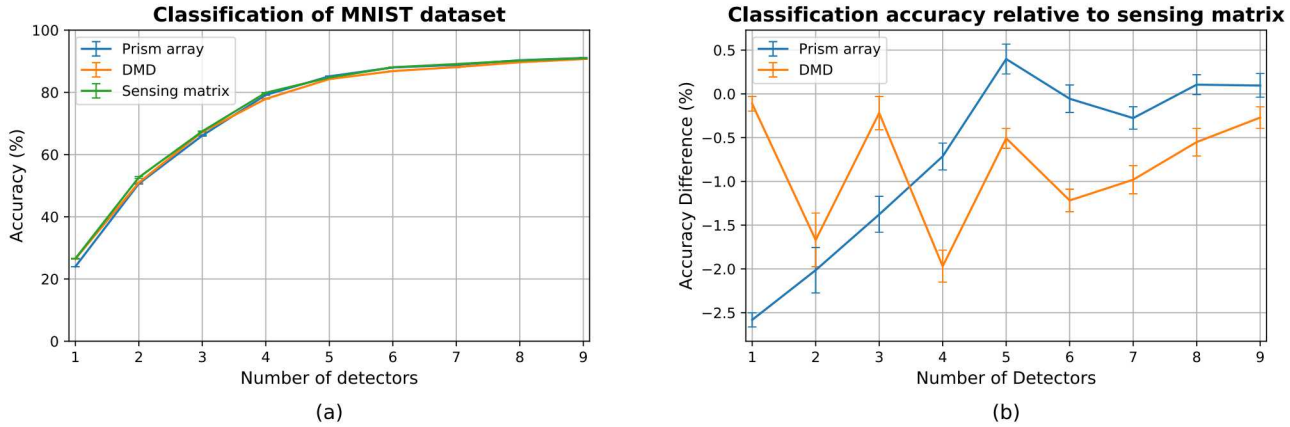

Figure 5. (a) The classification accuracy of the prism array architecture and the digital micromirror device (DMD) architecture had similar performance to the ideal sensing matrix as the number of detectors was increased. (b) The DMD architecture was slightly worse than the ideal sensing matrix for all the number of detector. The prism array architecture had performance exceeding the ideal sensing matrix for five, eight, and nine detectors.

To test the systems' tolerance to wavefront errors, aberrations were induced at the aperture plane of each system. The system response matrices were recorded for the nine detector configuration for 0, 0.25, 2, and 10 waves of spherical aberration, representing a range from zero aberrations to highly aberrated. Fig. 6 shows how the aberrations affected system performance. The performance of the DMD architecture decreases with increasing aberrations as was expected. The classification accuracy was greater than 85% even at 10 waves of spherical aberration. The induced aberration would not affect the channels equally because spherical aberration is more sever near the edge of the aperture. The outer channels would be tilted inwards, the transmission of the DMD would effectively be sampling different angles than those intended in the design.

The performance of the prism array showed no decrease with increasing aberrations. There was a slight increase in performance which was greater than the standard deviation of the measurements. The blurring in the system response matrix decreased the detrimental effect caused by spherical aberration.

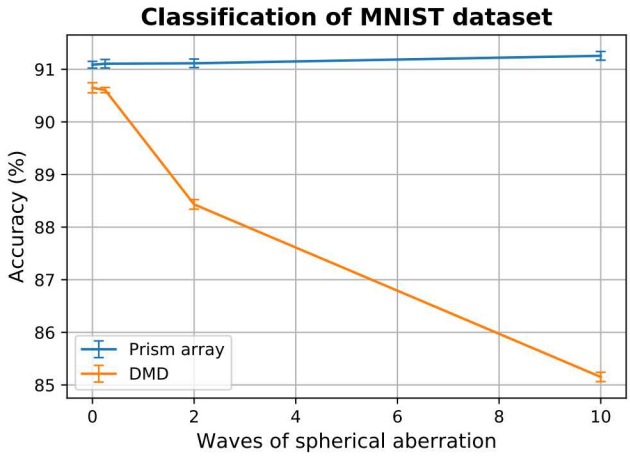

Figure 6. The digital micromirror device (DMD) architecture was much more sensitive to induced spherical aberration than the prism array architecture.

5. COMPARISON

The two compressive sensing architectures described in this paper are both realizations of the same sensing matrices; however, the architectures have different strengths and weaknesses. The prism array is a monolith element that requires specialized fabrication. The DMD architecture was much larger and required more power but the optics could be realized using off the shelf components and an easily fabricated prism array.

The construction of the two architectures have different challenges. The fabrication of the prism array requires specialize tools such as additive manufacturing. However, assembly of the system is trivial after the part is fabricated. The prism array has to be aligned to the detector elements. The overfill of the detectors allows for some misalignment, and the architecture has been shown to be highly resistant to aberrations such as defocus and spherical. The only custom components required for the DMD architecture are the nine prisms used to split the channels. All the other components can be realized with commercial off the shelf components, and the sensing matrix can be changed without changing the hardware. Assembling the system is more involved because it requires aligning seven elements, and it has been shown that the system is moderately sensitive to spherical aberration.

The form factor of the two systems is also a consideration. The prism array is designed to mount 10 mm in front of the detectors. The only external components needed would be to control the field of view. The DMD architecture is much larger because it requires optics to adjust the field of view and twice the objective focal length. Along with the horizontal space required for the relay lens and the detectors. Optimization can reduce the footprint, but the system will not reduce to the size of the prism array architecture.

From a throughput standpoint, the prism array makes more efficient use of the aperture area, but there is no magnification so the aperture area is limited by the prism area or the detector area, whichever is smaller. The DMD architecture can be optimized to increase the magnification increasing the effective area of detector at the aperture plane. From the radiometric model, the DMD architecture had a higher throughput. It should be noted that the blurring was not included in the effective field of view of the prism array architecture because it was assumed that the blurring would introduce noise. The classification performance indicated that blurring could possibly improve performance would result in the throughput of the prism array architecture being greater than calculated.

For errors in the sensing matrix, the DMD is capable of more faithful reproducing the sensing matrix. The only blurring was only from the aberration in optics which can be expected to be minimal. The objective lens has a one-to-one mapping of input angles, so no angle crosstalk was seen or is expected. If the spacing between the channels on the DMD is too narrow then overlapping channels will cause significant channel crosstalk. The prism array architecture blurs the sensing matrix, however the analysis of system performance indicated that the blurring does not decrease system performance. The blurring may increase classification accuracy and make the system less susceptible to aberrations.

6. CONCLUSION

We have presented two optical architectures for the creation of task-specific compressive imagers. The first architecture was a monolithic part that used a prism array to directly implement the sensing matrix. The second architecture used used a simple prism array, conventional optics, and a digital micromirror device (DMD) to implement the sensing matrix.

The radiometric throughput of both systems were found to be greater than an F/4 lens imaging onto 5 μm pixels. The sensing matrix of each architecture was simulated using non-sequential raytracing for configurations of detectors ranging from one to nine. The prism array was shown to blur the sensing matrix, where the DMD architecture was shown to reproduce the sensing matrix with much greater fidelity. However, the classification performance of the two systems was shown the be similar despite the blurring. Additionally, the prism array was shown to be less susceptible to aberrations, likely because of the blurred sensing matrix.

In the comparison between the two systems we discussed that the prism array architecture was more difficult to fabricate, but was monolithic and therefore a smaller device that is easier to assemble. The DMD architecture

has more degrees of freedom which allows for more optimization and is better for applications with a changing sensing matrix.

In future work we will explore the how the radiometric throughput effects system performance, and develop methods to optimize the designs for task-specific performance instead of classical metrics such as reducing aberration. We will also investigate how non-ideal optics affect the performance of the systems, and fabricate both architectures to compare simulated results to prototype performance.

7. ACKNOWLEDGMENTS

Supported by the Laboratory Directed Research and Development program at Sandia National Laboratories, a multimission laboratory managed and operated by National Technology and Engineering Solutions of Sandia, LLC., a wholly owned subsidiary of Honeywell International, Inc., for the U.S. Department of Energy's National Nuclear Security Administration under contract DE-NA-0003525.

REFERENCES

[1] Calderbank, R., Jafarpour, S., and Schapire, R., "Compressed learning: Universal sparse dimensionality reduction and learning in the measurement domain," *preprint* (2009).

[2] Lohit, S., Kulkarni, K., and Turaga, P., "Direct inference on compressive measurements using convolutional neural networks," *IEEE International Conference on Image Processing (ICIP)* , 1913–1917 (2016).

[3] Timofte, R. and Van Gool, L., "Sparse representation based projections," *Proceedings of the 22nd British machine vision conference-BMVC* , 61–1 (2011).

[4] Birch, G. C., Quach, T.-T., Galiardi, M., LaCasse, C. F., and Dagel, A. L., "Optical systems for task-specific compressive classification," (2018).

[5] Cireşan, D., Meier, U., Masci, J., and Schmidhuber, J., "Multi-column deep neural network for traffic sign classification," *Neural Networks* **32**, 333 – 338 (2012). Selected Papers from IJCNN 2011.

[6] Huval, B., Wang, T., Tandon, S., Kiske, J., Song, W., Pazhayampallil, J., Andriluka, M., Rajpurkar, P., Migimatsu, T., Cheng-Yue, R., Mujica, F., Coates, A., and Ng, A. Y., "An empirical evaluation of deep learning on highway driving," *CoRR* (2015).

[7] Levi, G. and Hassner, T., "Age and gender classification using convolutional neural networks," (June 2015).

[8] Vardasca, R., Vaz, L., and Mendes, J., [*Classification and Decision Making of Medical Infrared Thermal Images*], 79–104, Springer International Publishing, Cham (2018).

[9] Kumar, A., Kim, J., Lyndon, D., Fulham, M., and Feng, D., "An ensemble of fine-tuned convolutional neural networks for medical image classification," *IEEE Journal of Biomedical and Health Informatics* **21**, 31–40 (Jan 2017).

[10] Romero, A., Gatta, C., and Camps-Valls, G., "Unsupervised deep feature extraction for remote sensing image classification," *IEEE Transactions on Geoscience and Remote Sensing* **54**, 1349–1362 (March 2016).

[11] Maggiori, E., Tarabalka, Y., Charpiat, G., and Alliez, P., "Convolutional neural networks for large-scale remote-sensing image classification," *IEEE Transactions on Geoscience and Remote Sensing* **55**, 645–657 (Feb 2017).

[12] Candès, E. J. et al., "Compressive sampling," *Proceedings of the international congress of mathematicians* **3**, 1433–1452 (2006).

[13] Ashok, A., Baheti, P. K., and Neifeld, M. A., "Compressive imaging system design using task-specific information," *Applied optics* **47**(25), 4457–4471 (2008).

[14] Neifeld, M. A., Ashok, A., and Baheti, P. K., "Task-specific information for imaging system analysis," *J. Opt. Soc. Am. A* **24**, B25–B41 (Dec 2007).

[15] Davenport, M. A., Duarte, M. F., Wakin, M. B., Laska, J. N., Takhar, D., Kelly, K. F., and Baraniuk, R. G., "The smashed filter for compressive classification and target recognition," *International Society for Optics and Photonics Computational Imaging V* **6498**, 64980H (2007).

[16] Duarte-Carvajalino, J. M. and Sapiro, G., "Learning to sense sparse signals: Simultaneous sensing matrix and sparsifying dictionary optimization," *IEEE Transactions on Image Processing* **18**(7), 1395–1408 (2009).

[17] Elad, M., "Optimized projections for compressed sensing," *IEEE Transactions on Signal Processing* **55**(12), 5695–5702 (2007).

[18] Xu, J., Pi, Y., and Cao, Z., "Optimized projection matrix for compressive sensing," *EURASIP Journal on Advances in Signal Processing* **2010**(1), 560349 (2010).

[19] Li, G., Zhu, Z., Yang, D., Chang, L., and Bai, H., "On projection matrix optimization for compressive sensing systems," *IEEE Transactions on Signal Processing* **61**(11), 2887–2898 (2013).

[20] Xu, S., de Lamare, R. C., and Poor, H. V., "Distributed compressed estimation based on compressive sensing," *IEEE Signal Processing Letters* **22**(9), 1311–1315 (2015).

[21] [*Pseudo-random Prism Arrays for Lensless Computational Imagers*], Optical Society of America (2017).